Journal of Physics:
Complexity

PURPOSE-LED PUBLISHING™

PAPER • **OPEN ACCESS**

Weak periodic signal identification in low amplitude seismic waves based on chaotic oscillator

To cite this article: Nazmi Yılmaz and Mahmut Akıllı 2025 *J. Phys. Complex.* **6** 035001

View the article online for updates and enhancements.

You may also like

- Research on the Source Parameters and Scaling Relations of Earthquakes in Qinba Mountain and Its Adjacent Area
Y Zheng and W D Wang
- Passive Seismic Tomography as a Tool of Rock Burst Hazard Prognosis in Copper Ore Mine in Poland
Anna Barbara Gogolewska and Daria Smolak
- Seismic Station Quality Monitoring and Evaluation System in Indonesia
R S Yuliatmoko, M.T Gunawan, M Adi et al.

This content was downloaded from IP address 88.255.99.14 on 06/04/2026 at 13:39

Journal of Physics: Complexity

PAPER

Weak periodic signal identification in low amplitude seismic waves based on chaotic oscillator

Nazmi Yılmaz[1,*] and Mahmut Akıllı[2]

[1] Department of Physics, College of Sciences, Koç University, Istanbul, Turkey
[2] Medical Imaging Techniques Program, Vocational School, Istanbul Arel University, Istanbul, Turkey
[*] Author to whom any correspondence should be addressed.

E-mail: nayilmaz@ku.edu.tr

Keywords: Duffing oscillator system, weak periodic signals, scale index, seismic waves

OPEN ACCESS

RECEIVED
3 March 2025

REVISED
17 April 2025

ACCEPTED FOR PUBLICATION
27 June 2025

PUBLISHED
8 July 2025

Original content from this work may be used under the terms of the Creative Commons Attribution 4.0 licence.

Any further distribution of this work must maintain attribution to the author(s) and the title of the work, journal citation and DOI.

Abstract

This study aims to identify weak periodic or quasi-periodic signals within seismic data, as these low-amplitude signals provide valuable insights into seismic dynamics but are often masked by chaotic noise. To address this challenge, we employ a novel detection method based on the Duffing oscillator, a tool well-suited for analyzing complex, noisy systems. Applying this approach to seismic data from two moderate earthquakes, we successfully extract weak periodic and quasi-periodic signals embedded within the noise. The results reveal distinct signal patterns that reflect the dynamics of the fault segments associated with the analyzed earthquakes. These findings demonstrate the effectiveness of chaos-based methods in seismic signal detection and highlight their potential for improving real-time seismic monitoring and prediction. More broadly, this work contributes to the understanding of chaos and complexity in natural systems, offering new perspectives for the study of seismic activity.

1. Introduction

Signals with periodic or quasi-periodic behavior can be identified as weak periodic signals within time series data obtained from various dynamical systems. These noisy weak periodic signals [1–4] exhibit very low signal-to-noise ratios, and consequently have low amplitudes. However, their predictable and deterministic characteristics make them valuable for analyzing dynamical systems, particularly non-stationary signals such as seismic signals [5–7].

The Duffing chaotic oscillator is a powerful tool for identifying weak signals buried in significant white noise, especially in cases where the signal-to-noise ratio is very low. Conventional Duffing oscillator methods rely on a state transition principle in phase space where the Duffing oscillator is initially set at the chaos threshold by adjusting the base signal amplitude. When weak signals interact with the Duffing system at this threshold, the oscillator transitions to a state of periodicity, allowing the identification of weak periodic signals submerged in noise [8–11].

Techniques such as stochastic resonance have been used to enhance weak periodic signal detection by introducing optimal noise into the system, boosting signals that would otherwise remain undetectable [12, 13]. For example, a recent study investigated the role of potential-well shape in noise-boosted weak signal detection in fractional-order systems, showing that increased well-width can improve signal amplification [14]. A related approach, chaotic resonance [15–17], uses intrinsic and extrinsic chaotic fluctuations as effective noise sources for signal detection, which has proven useful for extracting weak periodic signals in seismic data. Recent advances in fractional-order chaotic systems have shown that intrinsic chaotic fluctuations can amplify weak signals without external noise or preprocessing, enhancing practical fault diagnosis [18]. A combination of chaotic oscillators, such as the van der Pol–Duffing oscillator, have also demonstrated utility in weak periodic signal detection [19–21]. Other recent works have underscored the importance of chaotic detection methods [22–26].

© 2025 The Author(s). Published by IOP Publishing Ltd

A novel detection method for weak periodic signals based on the scale index of the driven Duffing chaotic oscillator was recently proposed. This method numerically distinguishes between periodic and chaotic regions of the Duffing system [27] by calculating wavelet-based scale index parameters, quantifying the aperiodic nature of a signal on a 0-to-1 scale [28, 29]. Specifically, when the system exhibits periodic behavior, the scale index parameter approaches zero, while it remains positive near the chaos threshold. This approach enables automatic identification of weak signals embedded in the Duffing equation [30], with results visualized by plotting the scale index against frequency.

In seismic data analysis, where identifying weak periodic signals is essential for understanding seismic dynamics, this technique provides significant advantages, especially in the context of chaos theory and complex signal processing for real-time earthquake monitoring and prediction. In this work, we utilize this automated graphical method to continuous low-amplitude seismic signals, investigating the frequency characteristics of weak signals before and during an earthquake for the first time. We focus our investigation on the Istanbul and Düzce earthquakes [31], moderate-intensity and shallow events that occurred approximately two years apart along the North Anatolian strike-slip fault line near Istanbul [32]. Identifying weak periodic signals within these earthquakes holds significant importance since the probability of a large-magnitude earthquake striking along this fault line to the south of Istanbul within the next 23 years is around 48% [33]. This fault line is also unique in generating westward-directed earthquakes since the Erzincan earthquake (magnitude 7.9) in 1939, as evidenced by the latest events of Kocaeli (magnitude 7.4) and Düzce (magnitude 7.2) in 1999 [34]. Furthermore, the southeast branch of the Anatolian fault line, extending towards the Arabian Peninsula, experienced one of the most significant and devastating double earthquakes in recent memory, occurring in February 2023 [35].

Our method introduces a novel approach to weak signal detection that differs from techniques such as chaotic resonance and stochastic resonance, which rely on external noise and careful parameter tuning. While our approach also requires specific tuned parameters—such as a gain coefficient to scale the input signal for the Duffing equation appropriately—it does not depend on optimizing external noise or transforming signals into sinusoidal forms. By employing the scale index of the Duffing oscillator, we enable direct and automatic identification of weak periodic and quasi-periodic signals within complex, noisy datasets, including non-sinusoidal signals like those observed during the Istanbul earthquake. This makes the method especially effective for real-world seismic analysis, where signals often appear as transient impacts or irregular bursts.

The method proves highly effective at isolating weak signal components amidst broadband noise, offering clear advantages over conventional phase-space-based techniques. Its automated nature allows for efficient processing of continuous datasets, enhancing the accuracy and practicality of real-time seismic monitoring. Notably, while the Duffing oscillator responds to periodic structures, our scale index analysis can reveal fundamental frequencies in harmonic and impact-like signals. This capability provides a powerful new tool for detecting subtle periodic structures in seismic records, advancing our understanding of chaotic dynamics in seismic systems and potentially improving earthquake monitoring and prediction capabilities.

2. Method

2.1. Using Duffing oscillator for weak periodic signal identification

The nonlinear Duffing equation is an effective tool to construct an oscillator system at the threshold of chaos for weak periodic signal identification. The fundamental expression of the equation is [4, 27, 30, 36];

$$\frac{\mathrm{d}^2x}{\mathrm{d}t^2}+\delta\frac{\mathrm{d}x}{\mathrm{d}t}-x+x^3=\gamma\cos(t)+\text{input}. \tag{1}$$

Here δ is the damping coefficient, $x+x^3$ is the nonlinear restoring force, γ base signal amplitude, and $\gamma\cos(t)$ is the base signal, the *input* term represents the signal that is embedded to the Duffing chaotic oscillator.

To identify weak signals with different frequencies, the time variable in the equation (1) is expressed as $t=w_0\tau$ where w_0 the angular frequency reference value of the base signal and τ is the dimensionless, rescaled time variable dependent on w_0.

The equation is then expressed as;

$$\begin{aligned}\frac{\mathrm{d}y}{\mathrm{d}\tau}&=\dot{y}(\tau)=\omega_0\left[-\delta y+x-x^3+\gamma\cos(\omega_0\tau)+\text{input}\right]\\ \frac{\mathrm{d}x}{d\tau}&=\dot{x}(\tau)=\omega_0 y.\end{aligned} \tag{2}$$

In equation (2), if δ is kept constant, and γ varied, the state of the driven Duffing chaotic oscillator transitions from a periodic state to a chaotic state, and then to a large periodic state. The state of the Duffing

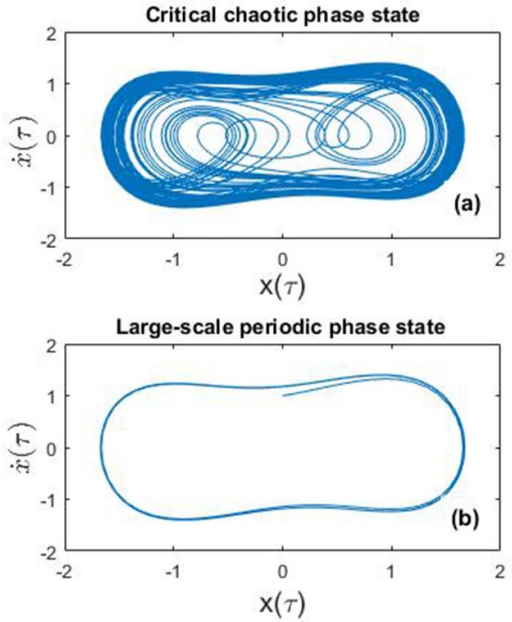


Figure 1. Duffing oscillator phase state diagrams; (a) The chaos threshold of the Duffing chaotic oscillator prior to the addition of the input term for $\gamma < \gamma_c$. (b) The periodic condition of the Duffing oscillator for $\gamma \geqslant \gamma_c$.

chaotic oscillator is governed by the bifurcation value γ_c which serves as the amplitude threshold for the transition from chaotic motion to large periodic motion is $\gamma = \gamma_c$. For $\gamma \geqslant \gamma_c$ Duffing chaotic oscillator is in a large periodic state, while for $\gamma < \gamma_c$, the oscillator remains in chaotic state [4, 27, 30]. This bifurcation value, γ_c is determined by solving equation (2) by the 4th-order Runge Kutta algorithm [37] and is dependent of the damping coefficient δ, time step size h, and the base signal angular frequency w_0. In the solution, $x(\tau)$ time series represent the computation results of equation (2) and $\dot{x}(\tau)$ is the derivative of $x(\tau)$. The resulting phase state diagram has $x(\tau)$ on the y-axis and $\dot{x}(\tau)$ on the x-axis.

In the context of identifying weak signals within a given input, the approach involves initially adjusting the Duffing oscillator to a phase state at the chaos threshold as demonstrated in figure 1(a) in the absence of any input signal. This adjustment is achieved through manipulation of the base signal amplitude, denoted as γ. The input signal is fed into the Duffing equation at chaos threshold, it transitions to a periodic state, as depicted in figure 1(b). This transition is evidence that the input signal contains weak signals. The Duffing oscillator transitions to state of periodicity only when the base signal frequency and the weak signal frequency are identical [4–9, 27]. Hence, the identified weak signals can exhibit either quasiperiodic or periodic behavior.

2.2. Identifying weak periodic signals using scale index tool and Duffing chaotic oscillator

In the pursuit of identifying the frequencies of weak signals within a given signal, conventionally, one would adjust the parameter w_0 in equation (2) while monitoring the phase state of individual numerical solutions of the Duffing oscillator. The objective is to detect a shift from the chaos threshold to periodicity.

To address the approach being not practical and time-intensive, we have formulated a more practical and efficient technique that combines the scale index with the Duffing oscillator [27, 30]. The scale index method has been used for measuring aperiodicity and can complement largest Lyapunov exponents for identifying chaos transitions in dynamical systems. It is derived from the wavelet transform. More specifically it is the ratio of the wavelet scalogram value at the dominant scale to the value at the least significant scale [28]. The continuous wavelet transform which provides the frequency components of a function $f(t)$ for a given scale and time is expressed as [38]:

$$Wf(u,s) = \langle f, \psi_{u,s} \rangle = \int_{+\infty}^{-\infty} f(t)\, \psi^*_{u,s}(t)\, \mathrm{d}t. \tag{3}$$

The energy of the continuous wavelet transform of $f(t)$ for individual scales in a given scale range is given by the wavelet scalogram:

$$S(s) = \|Wf(u,s)\| = \left(\int_{-\infty}^{+\infty} |Wf(u,s)|^2 du \right)^{1/2}. \tag{4}$$

The inner wavelet scalogram is used for the analysis of a finite time series [29]

$$S^{\text{inner}}(s) = \|Wf(u,s)\|_{J(s)} = \left(\int_{c(s)}^{d(s)} |Wf(u,s)|^2 du \right)^{1/2} \tag{5}$$

where $J(s)$ represents the maximum sub-interval within the selected finite time range that the wavelet function is supported in this time interval. The inner wavelet scalogram is normalized for obtaining scale independent scale index parameter [29];

$$\bar{S}^{\text{inner}}(s) = \frac{S^{\text{inner}}(s)}{(d(s) - c(s))^{\frac{1}{2}}}. \tag{6}$$

For a signal f, scale index in scales $[s_0, s_1]$ is expressed as;

$$i_{\text{scale}} = \frac{\bar{S}^{\text{inner}}(s_{\min})}{\bar{S}^{\text{inner}}(s_{\max})} \tag{7}$$

where $s_{\max}$ represents the minimum scale necessary for the normalized inner wavelet scalogram to reach maximum in the range of s_0 to s_1. And $s_{\min}$ denotes the minimum scale required for the normalized inner wavelet scalogram to go to minimum in the range of $s_{\max}$ to $2s_1$. As the scale index parameter increases from 0 to 1, indicating growing aperiodicity, it reflects the emergence of chaos within a system [29, 39–41].

The scale index method is integrated into the Duffing oscillator by computing the scale index parameters of the oscillator's numerical solutions. The resulting scale index spectrum for each oscillator frequency is plotted, allowing for the automatic detection of weak signals. Specifically, the scale index tends towards 0 when the oscillator settles into periodicity. Conversely, when the oscillator remains at the threshold of chaos, the scale index parameter exceeds 0. Consequently, by analyzing scale index parameters converging to zero, weak signal frequencies can be identified without the need for intricate phase space diagram analysis. Integrating the scale index method and the Duffing chaotic oscillator system significantly improves the identification of weak signals.

2.3. Identifying weak periodic signals in seismic waves

When seismic signals are used as input in equation (2), the damping coefficient δ is set to 0.5, which plays a critical role in the Duffing oscillator's dynamic behavior. At this value, the system transitions from chaotic to periodic dynamics when the cosine forcing amplitude exceeds approximately 0.826. This shift enhances the system's stability and predictability, improving its ability to isolate and amplify weak periodic signals from noisy seismic data. Thus, $\delta = 0.5$ corresponds to an optimized sensitivity state, facilitating reliable detection of subtle signal features [4, 27]. Under these conditions, the Duffing equation is expressed as:

$$\frac{\mathrm{d}^2x}{\mathrm{d}t^2} + 0.5\frac{\mathrm{d}x}{\mathrm{d}t} - x + x^3 = \gamma\cos(\omega_0\tau) + \text{input}[\tau]_{\text{seismic}}. \tag{8}$$

2.3.1. Scaling of the input signal

To effectively use the Duffing equation (8) for weak signal detection, the input signal must first be scaled to align with the numerical solution range of the Duffing oscillator based on empirical testing with respect to the term $\gamma\cos(\omega_0\tau)$. If the input signal amplitude is too large, the oscillator becomes unstable; conversely, if the signal is too small, it fails to stimulate the system. To resolve this, the input signal is adjusted using an empirically determined gain coefficient, making it one order of magnitude smaller than $\gamma\cos(\omega_0\tau)$ thus matching the oscillator's operational range [27, 30].

Since each seismic dataset can have unique noise characteristics, the gain coefficient may vary depending on the specific data characteristics and noise level. For instance, the seismic signal amplitude varies significantly during and before an earthquake, which necessitates different coefficient values. This empirical testing approach ensures that the input signal is adequately scaled to facilitate accurate weak signal detection within the chaotic system.

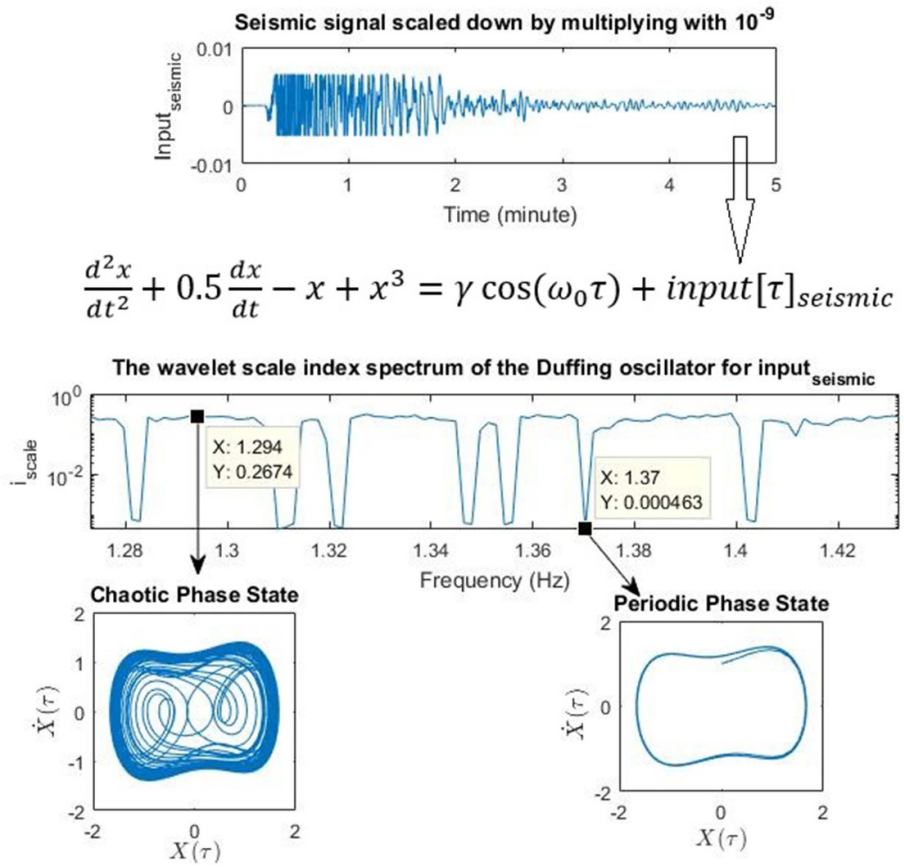


Figure 2. Visual representation of the analytical process of the automated weak periodic signal detection from seismic signals using the wavelet scale index spectrum of the Duffing oscillator.

2.3.2. Synchronizing the sample frequencies

Second, the Duffing oscillator sample frequency, f_{D} must match the input signal sample frequency f_{input} to ensure accurate synchronization between the oscillator and the input signal. To solve the Duffing equation numerically, the step size must be determined as $h = \frac{100}{f_{\mathrm{D}}}$ [27, 30]. For seismic signals as input, we set the Duffing oscillator sample frequency to $f_D = 500\,\mathrm{Hz}$ and the seismic data sample frequency to $f_{\mathrm{seismic}} = 50\,\mathrm{Hz}$. The input sample frequency was scaled to $f_{\mathrm{input}} = 10.f_{\mathrm{seismic}} = 10 \times 50 = 500\,\mathrm{Hz}$. Then, frequencies of weak signals identified in the seismic data were scaled by $\frac{f_{\mathrm{input}}}{f_{\mathrm{seismic}}} = 10$, Using the 4th-order Runge–Kutta method, the Duffing equation (8) was solved numerically with the step size $h = \frac{100}{f_{\mathrm{D}}} = \frac{100}{500} = 0.2$. The reference signal amplitude γ was adjusted to be just next to the bifurcation threshold γ_{c} before adding the seismic signal to the Duffing equation (8). Consequently, the weak signal amplitudes were estimated as $\gamma_{\mathrm{WPS}} \geqslant \gamma_{\mathrm{c}} - \gamma$.

2.3.3. Frequency scan and weak signal detection

We performed weak signal frequency scan within the interval of $0.508 \leqslant \omega_0 \leqslant 3.2$, iterating w_0 in steps of 0.001. For each angular frequency in this range, we computed the scale index values using equation (8). The computation employed the Haar wavelet with scales ranging from $s_0 = 1$ and $s_1 = 1024$. The angular frequency ω_0 and frequency f in the Duffing oscillator are related by $f = \frac{100\omega_0}{2\pi} = 10f_{\mathrm{seismic}}$. Based on this relationship, the seismic frequencies f_{seismic} correspond to the range from 0.8 Hz–5.1 Hz. Within this range, weak periodic (or quasi-periodic) signals were identified in the seismic data, characterized by scale index values $i_{\mathrm{scale}} < 10^{-2}$. Although seismic signals often contain impulsive rather than purely sinusoidal components, the proposed method remains effective. The Duffing oscillator with scale index detects synchronization with dominant repeating features—whether sine-like or composed of transient bursts—by identifying shifts in the underlying dynamics from chaos to periodicity. Figure 2 provides the visual representation of the analytical process, outlining the key steps and components involved in the methodology.

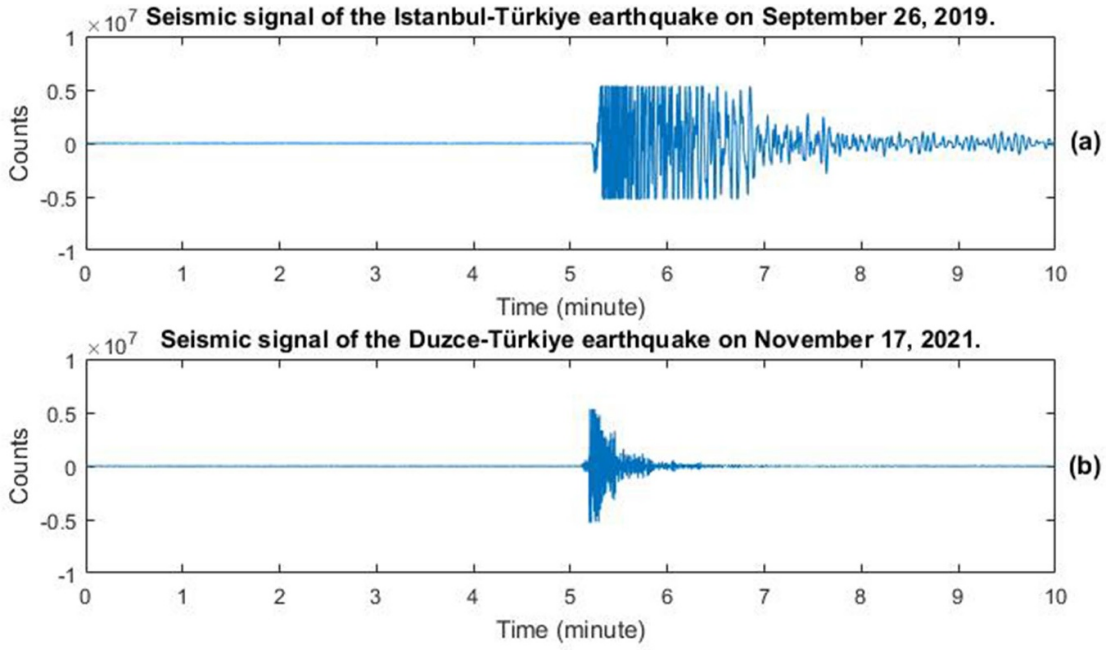


Figure 3. Seismic wave time series of Istanbul-Turkey, 26, 09, 2019 (magnitude 5.7) and Düzce, Turkey, 17, 11, 2021 (magnitude 5.2) earthquakes [32]. Reproduced with permission from [32]. © Boğaziçi University Kandilli Observatory and Earthquake Research Institute (KOERI).

3. Seismic data

Seismic data for this study was obtained from the Boğazici University Kandilli Observatory and Earthquake Monitoring Centre (www.koeri.boun.edu.tr/) [32]. We analyzed 10-minute segments of data for two moderate earthquakes, covering the 5 min before and after each event.

The first dataset corresponds to the Istanbul earthquake on 26 September 2019 (magnitude 5.7, depth 7 km), with an epicenter at 40.89° N, 28.17° E. Velocity-time data was recorded at the Silivri station (41.23° N, 28.21° E), located 37.9 km from the epicenter. Figure 3(a) presents the time series of this event.

The second dataset corresponds to the Düzce earthquake on 17 November 2021 (magnitude 5.2, depth 7.9 km), with an epicenter at 40.83° N, 31.02° E. Velocity-time data was recorded at the Mudurnu station (40.47° N, 31.19° E), situated 42.5 km from the epicenter. Figure 3(b) shows the time series for this event.

Düzce earthquake took place about two years after Istanbul earthquake. Their epicenters are relatively close at 239 km along the unique and notorious north Anatolian fault line as shown in figures 4 and 5. Both earthquakes are shallow with depths lower than <60 km and at moderate intensity category with $5.0 \leqslant$ magnitude $\leqslant 5.9$.

4. Results

Using the methodology outlined in section 2.3.3, we scanned the seismic signals in the angular frequency range $0.508 \leqslant \omega_0 \leqslant 3.2$, corresponding to the seismic frequencies f_{seismic} in the range 0.8 Hz–5.1 Hz.

Increasing the angular frequency w_0 also increases the bifurcation value γ_c in the Duffing chaotic oscillator. Therefore, the amplitude values γ in equation (8) were chosen as shown in table 1. We then computed the scale index values in equation (8) for the determined angular frequency range.

As shown in figures 6 and 7; low amplitude seismic data time series just before Istanbul and Düzce earthquakes were reduced in magnitude using a coefficient of 2.5 10^{-7} to fit the Duffing equation. By using this coefficient in inverse scaling; the amplitudes of the identified weak signals are:

$$\gamma_{\text{WPS}} \geqslant (\gamma_c - \gamma)/2.5 * 10^{-7} \geqslant (0.825571 - 0.82557).4 * 10^{6} \geqslant 4\,\text{counts}.$$

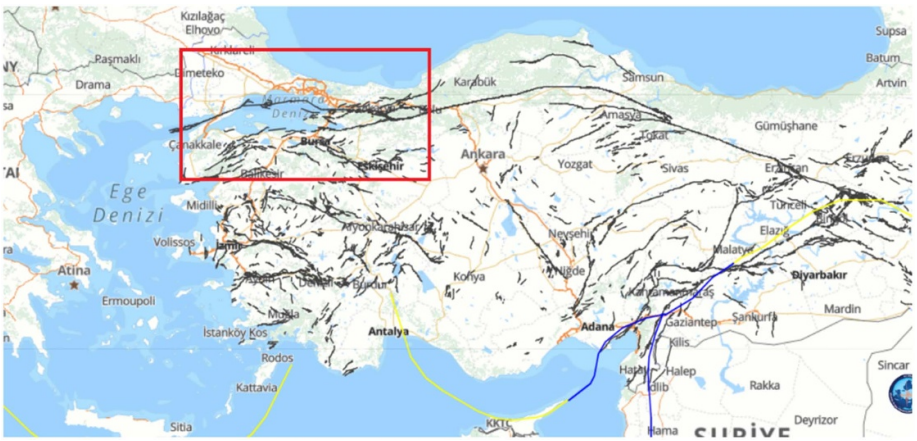


Figure 4. Eastern Mediterranean region showing the fault lines in Anatolia. The rectangle denotes the study region west of the North Anatolian fault line [32]. Reproduced with permission from [32]. © Boğaziçi University Kandilli Observatory and Earthquake Research Institute (KOERI).



Figure 5. The closer look at the study area, the Marmara Sea region, with the locations of Istanbul-Turkey, 26, 09, 2019 (magnitude 5.7) and Düzce, Turkey, 17, 11, 2021 (magnitude 5.2) earthquakes represented by the two circles [32]. Reproduced with permission from [32]. © Boğaziçi University Kandilli Observatory and Earthquake Research Institute (KOERI).

Table 1. Selected amplitude values for Istanbul and Düzce earthquakes seismic data in the range of $0.508 \leqslant w_0 \leqslant 3.200$.

$w_0$range	γ	γ_c
$0.508 \leqslant w_0 \leqslant 0.701$	0.825 55	0.825 56
$0.702 \leqslant w_0 \leqslant 0.813$	0.825 56	0.825 563
$0.814 \leqslant w_0 \leqslant 0.923$	0.825 563	0.825 565
$0.924 \leqslant w_0 \leqslant 1.090$	0.825 565	0.825 567
$1.091 \leqslant w_0 \leqslant 1.380$	0.825 567	0.825 569
$1.381 \leqslant w_0 \leqslant 1.646$	0.825 569	0.825 57
$1.647 \leqslant w_0 \leqslant 2.146$	0.825 57	0.825 571
$2.147 \leqslant w_0 \leqslant 3.200$	0.825 571	0.825 572

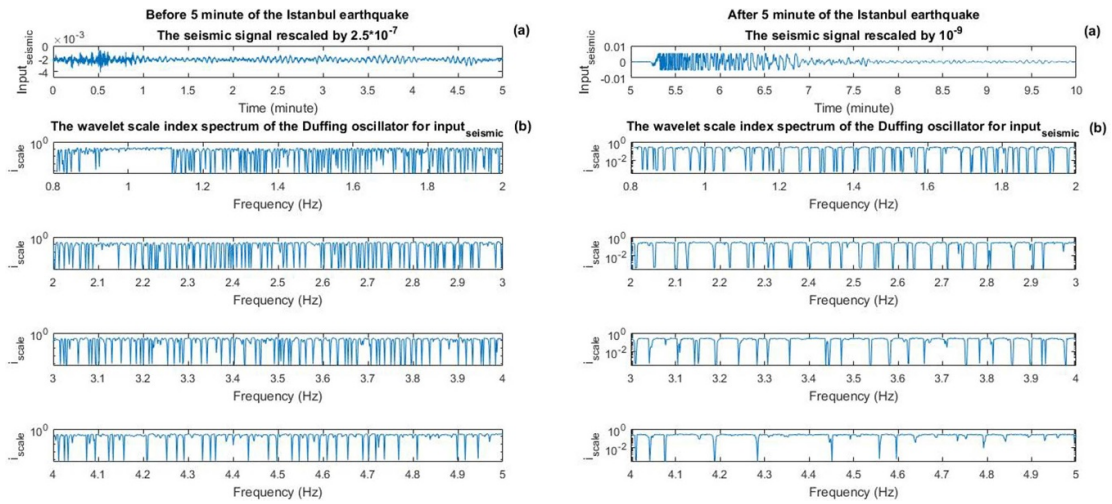


Figure 6. (a) The series of seismic wave durations 5 min before (**left**) and after (**right**) the Istanbul earthquake have been rescaled by 2.5 10^{-7} and 10^{-9} respectively. (b) The Duffing chaotic oscillator wavelet scale index spectrum for seismic wave time series just before (**left**) and after (**right**) Istanbul earthquake. Scale index values lower than $i_{\text{scale}} < 10^{-2}$ indicate the frequencies of weak periodic (or quasi-periodic) signals identified in this seismic signal.

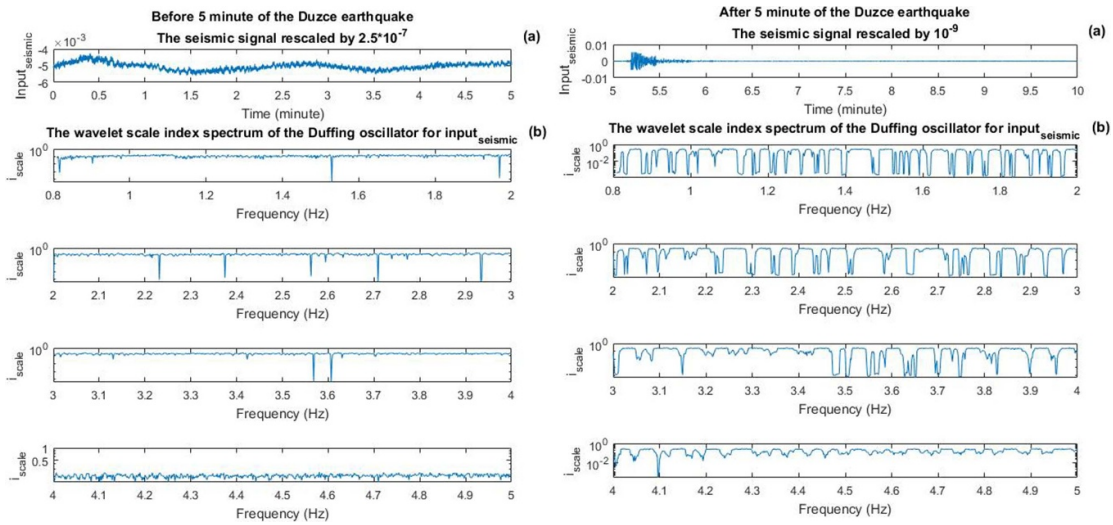


Figure 7. (a) The series of seismic wave durations 5 min before (**left**) and after (**right**) the Duzce earthquake have been rescaled by 2.5 10^{-7} and 10^{-9} respectively. (b) The Duffing chaotic oscillator wavelet scale index spectrum for seismic wave time series just before (**left**) and after (**right**) Duzce earthquake. Scale index values lower than $i_{\text{scale}} < 10^{-2}$ indicate the frequencies of weak periodic (or quasi-periodic) signals identified in this seismic signal.

Istanbul and Duzce earthquakes seismic data time series were fitted to the Duffing equation via scaling down by a gain coefficient of 10^{-9} to fit the Duffing equation. The amplitudes of the identified weak signals are:

$$\gamma_{\text{WPS}} \geqslant (\gamma_c - \gamma)/10^{-9} \geqslant (0.825571 - 0.82557).10^{9} \geqslant 1000\,\text{counts}.$$

We can then calculate the ratio of weak signal (W) to seismic signal (S), using the seismic-to-weak-signal ratio (SWR);

$$(\gamma_{\text{WPS}})_{\text{before}} = 4\ \text{counts}, (\gamma_{\text{WPS}})_{\text{after}} = 1000\ \text{counts}$$

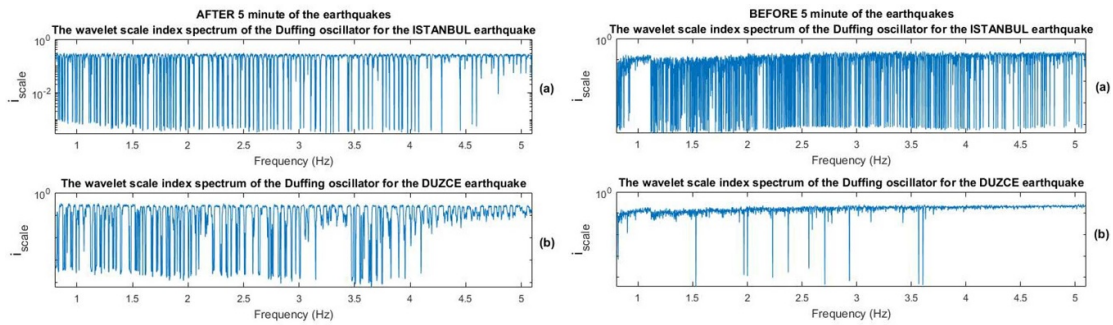


Figure 8. The Duffing chaotic oscillator wavelet scale index spectrum for seismic wave time series just before (**left**) and after (**right**) the earthquakes. Scale index values lower than $i_{\text{scale}} < 10^{-2}$ indicate the frequencies of weak periodic (or quasi-periodic) signals identified in this seismic signal.

Root mean square values of the seismic data:

$$\text{Before the Istanbul earthquake: } (\text{ist1})_{\text{rms}} = 8.74710^{3} \text{ counts}$$
$$\text{After the Istanbul earthquake: } (\text{ist2})_{\text{rms}} = 2.19210^{6} \text{ counts}$$
$$\text{Before the Düzce earthquake: } (\text{duz1})_{\text{rms}} = 2.01910^{4} \text{ counts}$$
$$\text{After the Düzce earthquake: } (\text{duz2})_{\text{rms}} = 6.46510^{5} \text{ counts}$$

$$\text{SWR}_{\text{ist1}} = 10\log_{10}\left(0.5\frac{\left((\gamma_{\text{WPS}})_{\text{before}}{}'\right)^{2}}{\left((\text{ist1})_{\text{rms}}\right)^{2}}\right) = -69.81 \text{ db}$$

$$\text{SWR}_{\text{ist2}} = 10\log_{10}\left(0.5\frac{\left((\gamma_{\text{WPS}})_{\text{after}}\right)^{2}}{\left((\text{ist2})_{\text{rms}}\right)^{2}}\right) = -69.83 \text{ db}$$

$$\text{SWR}_{\text{duz1}} = 10\log_{10}\left(0.5\frac{\left((\gamma_{\text{WPS}})_{\text{before}}{}'\right)^{2}}{\left((\text{duz1})_{\text{rms}}\right)^{2}}\right) = -77.07 \text{ db}$$

$$\text{SWR}_{\text{duz2}} = 10\log_{10}\left(0.5\frac{\left((\gamma_{\text{WPS}})_{\text{after}}\right)^{2}}{\left((\text{duz2})_{\text{rms}}\right)^{2}}\right) = -59.22 \text{ db}.$$

These results indicate that the detection efficiency of the method exhibits a threshold with respect to SWR, beyond which the efficiency declines [30]. This suggests that when the weak signal is too deeply embedded in noise, the method's ability to detect it diminishes, highlighting a limitation in high-noise environments. Further optimization for varying noise conditions may enhance the method's real-world applicability in earthquake monitoring systems. Moreover, the Duffing oscillator's sensitivity to parameter variations—such as the damping coefficient (δ) and the gain coefficient—also plays a critical role in detection performance. Deviations from optimal values may reduce the oscillator's responsiveness to weak signals. Additionally, environmental noise and external disturbances can perturb the oscillator's nonlinear dynamic behavior, further affecting detection reliability. These factors underscore the importance of robust parameter tuning and system calibration for practical deployment.

Figure 8 summarizes the measurements, highlighting key trends within the frequency range of 0.8 Hz–5 Hz. First, the number of weak periodic signals in the low-amplitude seismic waves preceding the Istanbul earthquake was higher than those before the Duzce earthquake. Second, we observed a notable absence of weak periodic signals in the frequency range of 0.9 Hz–1.2 Hz prior to both earthquakes. This absence was not evident in the seismic signals recorded during and immediately after the earthquakes. Additionally, we found that for both earthquakes, the number of weak periodic signals decreased significantly above approximately 4 Hz, which is consistent with the expected frequency range of an earthquake.

The number of weak periodic signals during and immediately following the seismic events is noticeably higher than those in the low-amplitude seismic activity before the earthquakes. This discrepancy can be attributed to the significant difference in the detection precision: weak signals were detected with $\geqslant 4$ counts for low-amplitude waves before the earthquake and $\geqslant$1000 counts during and immediately after the earthquake. Consequently, weak periodic signals were far more prevalent during and immediately after the seismic events than in the low-amplitude seismic waves preceding them. This shows that determining the detection precision for a signal is an important factor in interpreting the results of the method. These

findings underline the distinct dynamics of seismic activity in different temporal stages of an earthquake and highlight the potential of the proposed methodology in characterizing seismic signals.

5. Discussion

In this paper, we presented a novel weak periodic signal identification technique rooted in wavelet scale index analysis of the driven Duffing chaotic oscillator, adapting it to the analysis of low-amplitude seismic signals. This new methodology allowed us to effectively isolate weak periodic signals embedded within seismic data from Istanbul and Düzce earthquakes, two moderate-intensity and shallow events approximately two years apart along the North Anatolian strike-slip fault line near Istanbul. We gained deeper insights into the complex and chaotic dynamics underlying these seismic events by identifying and analyzing weak signals.

Our findings highlight key differences in the weak periodic signal patterns preceding and during the two earthquakes, reflecting the distinct dynamics of their respective fault line segments. The low-amplitude seismic waves preceding the Istanbul earthquake showed a higher abundance of weak periodic signals. This could be due to the Istanbul earthquake occurring on a more active segment of the North Anatolian Fault, compared to the segment near Düzce, which had experienced two major earthquakes in 1999 [33], potentially influencing the observed signal patterns. Additionally, the absence of weak periodic signals in the 0.9 Hz to 1.2 Hz range before both earthquakes is intriguing, as typical seismic waves usually encompass this frequency range. The significant signal decline above 4 Hz during the earthquakes aligns with the expected frequency characteristics of seismic events.

By comparing the two earthquakes, we were able to differentiate between them based on the abundance of weak periodic signals detected. Specifically, there was a higher number of weak signals before and during the Istanbul earthquake than the Düzce earthquake. This finding aligns with seismic assessments of the earthquakes, confirming that the Istanbul earthquake occurred along the North Anatolian main fault line, while the Düzce earthquake occurred along a smaller branch of the main fault [32]. Notably, the main fault line near Düzce had previously experienced a major earthquake of magnitude 7.2 in August and November of 1999.

Consequently, this automated approach offers clear advantages over conventional phase space analysis in identifying weak signals, especially in noisy, real-world datasets. It is computationally efficient and well-suited for integration into real-time earthquake monitoring systems due to its ability to process continuous seismic records. This opens new possibilities for early warning systems, where subtle periodic signals may serve as precursors to major seismic events. In practical applications, the method can complement existing seismological tools and be deployed in regional monitoring networks with modest computational resources. It presents promising avenues for future research in seismic monitoring and earthquake prediction, especially when combined with other weak signal detection techniques, such as chaotic resonance. Future studies will apply this method across a broader range of earthquake magnitudes and geographical locations to validate its global applicability. By continuing to explore the chaotic nature of seismic waves with tools like the Duffing oscillator, we aim to advance both the theoretical framework and practical implementation of chaos-based seismic monitoring systems.

Data availability statement

The data that support the findings of this study are openly available at the following URL/DOI: www.koeri.boun.edu.tr/.

CRediT authorship contribution statement

Nazmi Yılmaz: Writing—review & editing, Writing—original draft, Methodology, Investigation, Formal analysis, Conceptualization.

Mahmut Akıllı: Writing—review & editing, Methodology, Investigation, Formal analysis.

Conflict of interest

The authors have no competing interests to declare that are relevant to the content of this article.

Funding statement

No funding was received for this work.

References

[1] Li G, Tan N and Li X 2020 Weak signal detection method based on the coupled Lorenz system and its application in rolling bearing fault diagnosis *Appl. Sci.* **10** 4086
[2] Wang Q B, Yang Y and Zhang X 2020 Detection of weak signal based on parameter identification of delay differential system with noise disturbance *Math. Probl. Eng.* **2020** 2047952
[3] Luo J, Xu X, Ding Y, Yuan Y, Yang B, Sun K and Yin L 2018 Application of a memristor-based oscillator to weak signal detection *Eur. Phys. J. Plus* **133** 239
[4] Wang G, Chen D, Lin J and Chen X 1999 The application of chaotic oscillators to weak signal detection *IEEE Trans. Ind. Electron.* **46** 440–4
[5] Li Y, Yang B J, Zhao X P, Zhang M and Lin H B 2005 Algorithm of chaotic vibrator to detect weak events in seismic prospecting records *Chin. J. Geophys.* **48** 1502–8
[6] Li Y, Yang B J, Badal J, Zhao X P, Lin H B and Li R L 2009 Chaotic system detection of weak seismic signals *Geophys. J. Int.* **178** 1493–522
[7] Sun M, Li Z, Li Z, Li Q, Liu Y and Wang J 2020 A noise attenuation method for weak seismic signals based on compressed sensing and CEEMD *IEEE Access* **8** 71951–64
[8] Wang G Y and He S L 2003 A quantitative study on detection and estimation of weak signals by using chaotic Duffing oscillators *IEEE Trans. Circuits Syst. I* **50** 945–53
[9] Li G, Zeng L, Zhang L and Wu Q M J 2018 State identification of Duffing oscillator based on extreme learning machine *IEEE Signal Process. Lett.* **25** 25–29
[10] Luo W M and Zhang Y R 2018 Non-periodic pulse signal detection based on variable scale coupled Duffing oscillators *Electron. Lett.* **54** 280–1
[11] Akıllı M 2016 Detecting weak periodic signals in EEG time series *Chin. J. Phys.* **54** 77–85
[12] Asdi A S and Tewfik A H 1995 Detection of weak signals using adaptive stochastic resonance *1995 Int. Conf. on Acoustics, Speech, and Signal Processing* (*Detroit, MI, USA*) vol 2 pp 1332–5
[13] Moss F, Ward L M and Sannita W G 2004 Stochastic resonance and sensory information processing: a tutorial and review of application *Clin. Neurophysiol.* **115** 267–81
[14] Qiao Z, He Y, Liao C and Zhu R 2023 Noise-boosted weak signal detection in fractional nonlinear systems enhanced by increasing potential-well width and its application to mechanical fault diagnosis *Chaos Solitons Fractals* **175** 113960
[15] Nobukawa S, Nishimura H, Yamanishi T and Liu J-Q 2015 Analysis of chaotic resonance in Izhikevich neuron model *PLoS One* **10** e0138919
[16] Nobukawa S, Nishimura H and Yamanishi T 2017 Chaotic resonance in typical routes to chaos in the Izhikevich neuron model *Sci. Rep.* **7** 1331
[17] Baysal V, Saraç Z and Yilmaz E 2019 Chaotic resonance in Hodgkin–Huxley neuron *Nonlinear Dyn.* **97** 1275–85
[18] He Y, Fu Y, Qiao Z and Kang Y 2021 Chaotic resonance in a fractional-order oscillator system with application to mechanical fault diagnosis *Chaos Solitons Fractals* **142** 110536
[19] Zhihong Z and Yang S 2015 Application of van der Pol–Duffing oscillator in weak signal detection *Comput. Electr. Eng.* **41** 1–8
[20] Peng H-H, Xu X, Yang B-C and Yin L-Z 2016 Implication of two-coupled differential Van der Pol duffing oscillator in weak signal detection *J. Phys. Soc. Japan* **85** 8
[21] Wang K, Yan X, Yang Q, Hao X and Wang J 2020 Weak signal detection based on strongly coupled Duffing-Van der Pol oscillator and long short-term memory *J. Phys. Soc. Japan* **89** 014003
[22] Yang H, Liu B A and Li G H 2024 High-order double-coupled Duffing oscillator system with additional damping term and its application in ship-radiated noise signal detection *Eur. Phys. J. Plus* **139** 662
[23] Li G H, Xie R T and Yang H 2024 Study on fractional-order coupling of high-order Duffing oscillator and its application *Chaos Solitons Fractals* **186** 115255
[24] Shen Y P, Li Y A, Li W J, Gao H and Wu C 2024 A novel underwater weak target detection method based on 3D chaotic system and maximal overlap discrete wavelet transform *Eur. Phys. J. Plus* **139** 325
[25] Li G H, Liu F and Yang H 2024 A new detection model of ship-radiated noise signal *Ocean Eng.* **297** 117081
[26] Li G H, Xie R T and Yang H 2024 Dynamic analysis of the fractional-order Duffing-Van der Pol oscillator and its application extension *Nonlinear Dyn.* **112** 17709–32
[27] Akıllı M and Yılmaz N 2018 Study of weak periodic signals in the EEG signals and their relationship with postsynaptic potentials *IEEE Trans. Neural Syst. Rehabil. Eng.* **26** 1918–25
[28] Benitez R, Bolos V J and Ramirez M E 2010 A wavelet based tool for studying non-periodicity *Comput. Math. Appl.* **60** 634–41
[29] Bolós V J, Benítez R, Ferrer R and Jammazi R 2017 The windowed scalogram difference: a novel wavelet tool for comparing time series *Appl. Math. Comput.* **312** 49–65
[30] Akilli M, Yilmaz N and Akdeniz K G 2020 Automated system for weak periodic signal detection based on Duffing oscillator *IET Signal Process.* **14** 710–6
[31] Yılmaz N, Akıllı M and Ak M 2023 Temporal evolution of entropy and chaos in low amplitude seismic wave prior to an earthquake *Chaos Solitons Fractals* **173** 113585
[32] Bogazici University Kandilli Observatory and Earthquake Monitoring Center (KOERI) Regional Earthquake-Tsunami monitoring Center (RETMC). Earthquake data archive (available at: www.koeri.boun.edu.tr/) (March 2022, April 2023)
[33] Murru M, Akinci A, Falcone G, Pucci S, Console R and Parsons T 2016 M $\geqslant$ 7 earthquake rupture forecast and time-dependent probability for the sea of Marmara region, Turkey *J. Geophys. Res. Solid Earth* **121** 2679–707
[34] Licciardi A, Eken A T, Taymaz T, Piana N, Agostinetti V and Yolsal-Çevikbilen S 2018 Seismic anisotropy in central North Anatolian fault zone and its implications on crustal deformation *Phys. Earth Planet. Inter.* **277** 99–112
[35] Dal Zilio D, L and Ampuero J P 2023 Earthquake doublet in Turkey and Syria *Commun. Earth Environ.* **4** 71
[36] Kovacic I and Brennan M J 2011 *The Dufing Equation: Nonlinear Oscillators and Their Behaviour* (Wiley)
[37] Griffiths D F and Higham D J 2010 *Numerical Methods for Ordinary Differential Equations* (Springer)
[38] Mallat S 1999 *A Wavelet Tour of Signal Processing* (Academic)
[39] Yılmaz N, Canbaz B, Akıllı M and Önem C 2018 Study of the stability of the fermionic instanton solutions by the scale index method *Phys. Lett. A* **382** 2118–21
[40] Yılmaz N 2021 Characterizing the aperiodic behavior of seismic waves using the scale index analysis *Arab. J. Geosci.* **14** 2063
[41] Akıllı M, Yılmaz N and Akdeniz K G 2019 Study of the q-gaussian distribution with the scale index and calculating entropy by normalized inner scalogram *Phys. Lett. A* **383** 1099–104